75th International Astronautical Congress (IAC), Milan, Italy, 14-18 October 2024.

IAC-24-D4.IPB.17

Beyond the Limits – Arbitrarily Large Rotating Space Habitats through Structural Decoupling

Elliott Orion Ruzicka[a]

[a] *Orbital Design*, *311 E 3rd Street, New York, NY, 10009, USA,* orion@orbital.design

Abstract

Rotating space habitats have been a staple of space habitat design language since Tsiolkovsky's writings dating back to 1903. The notional conception of a rotating space habitat has a maximum theoretical size, which is due to the breaking length of the structural material. While this notional rotating space habitat concept has been universally assumed, it has a glaring design flaw: the structural mass contributes to the centrifugal weight. This flaw inherently limits the structural mass efficiency of the habitat and is solely responsible for the oft-cited maximum theoretical size. Although it might seem unavoidable, the limitations associated with this flaw are not intrinsic to the concept of rotating habitats and can be overcome. This study proposes a novel design solution: decouple the habitat and structure, enabling the habitat to function as a rotating inner ring encased within a static structural ring. By keeping the structural ring static, it need not resist the centrifugal force generated by its own mass, ensuring that the structural mass does not contribute to additional hoop stress. This research focuses on the application of superconducting magnetic levitation of the inner, rotating ring against the outer, static ring, thereby substantially diminishing the hoop stress on the outer ring. The core objective of this research is to validate the hypothesis that decoupling the rotating portion of the habitat from the support structure eliminates size constraints associated with rotating habitats and decreases the amount of structural material required. This validation is achieved through theoretical proofs as well as practical model experimentation, each of which illustrate the fundamental principles. Consequently, this allows for the construction of extremely large habitats using rudimentary materials, challenging the predominant view that advanced materials are necessary for such structures. Such a habitat would maintain additional benefits, such as kinetic energy storage and straightforward docking/berthing. The results of this research have immediate implications for reducing the structural mass of prospective rotating space habitat designs and opens possibilities for using common materials in large-scale habitat construction. Given these outcomes, the findings not only pave the way for more efficient and sustainable space habitat construction but also signal a pivotal shift in the field. This research lays the groundwork for a comprehensive re-evaluation of rotating habitat design, underscoring the need for further exploration in areas such as the development of orbital test beds for magnetic levitation, biological testing across different gravity levels, and comparative analyses of structural materials.

Keywords: (space habitat, rotating habitat, artificial gravity, breaking length)

Nomenclature

σ_θ	Hoop stress
p	Pressure
r	Radius
t	Thickness
m	Mass
a	Acceleration
L	Angular momentum
I	Moment of inertia
ω	Rotational velocity
F_{tu}	Ultimate tensile strength

Subscripts

$_s$	Structure
$_h$	Habitat

Acronyms/Abbreviations

YBCO	Yttrium Barium Copper Oxide
NFC	Null Flux Coil
PWM	Pulse Width Modulation
RPM	Revolutions Per Minute

1. Introduction

1.1 Background

Rotating habitats have been a staple of speculative space habitat design since the beginning of the discipline of space design in the 1960s, and even before then in the works of Tsiolkovsky, Bernal, and von Braun. At a rudimentary level, artificial gravity can be intuitively understood as the same phenomenon that keeps water in a bucket when swung over one's head [1]; rotating habitats do the same thing in space to impart the sensation of gravity to the occupants. Conceptual designs of rotating habitats vary widely, whether depicted in concept art, speculative fiction, or even research papers. While the sizes, shapes, and configurations of these designs may be quite different, they share one commonality: there is a limit to how large they can plausibly be.

1.2 Limitations in Conceptual Designs

Some of the earliest work in actual rotating space habitat design originated with Tsiolkovsky, Potočnik, and von Braun in their concepts for rotating space habitats [2, 3, 4], which undoubtedly inspired fictional works such as *2001: A Space Odessey* [5], noted for their simple, foundational design and human scale. These designs succeeded at providing a schematic proof of concept that was unassailable from a structural standpoint due to the limited scale proposed.

In the 1975 NASA Summer Study conducted at Stanford University, various concepts were put forward for rotating space habitat concepts. These included the eponymous Stanford Torus, the Bernal Sphere (proposed earlier by Bernal), and what would be later known as the O'Neill Cylinder [6]. Despite capturing the imagination of generations to come, and despite their ambitious scale, they were all sized based on an understanding of the physical limitations of structural materials; no concept was put forth that was not feasible from a structural standpoint. So, while impressive when compared to earlier conceptions for space-station-scale rotating space habitats of Tsiolkovsky, Potočnik, and von Braun, the summer study concepts were all limited in size.

Several fictional works portray rotating space habitats at various scales, but few are as well-known or immense as the Banks Orbital (*The Culture* series by Iain M. Banks [7]) and the even larger Ringworld (*Ringworld* series by Larry Nivin [8]). While these concepts are cosmetically similar (an open-air, ring-shaped habitat), they differ greatly in their scale and their justifications to support it. A Banks Orbital can be as modest as a thousand kilometers to millions of kilometers in diameter. Canonically, these structures are held together via fictional force fields rather than structural material. In the case of the Ringworld, it is hundreds of millions of kilometers in diameter. Rather than force fields, the Ringworld is held together by a fictional material called Scrim, a material stronger by far than any material known or conceived of by humankind. The authors of these stories knew of the structural limitations of rotating space habitats, so they inserted advanced fictional technology to add verisimilitude to their stories.

All these examples share the acknowledgement that rotating space habitats have a maximum allowable size. This maximum size is a property of the structural material and is known as the breaking length (see section 3.4.1).

2. Theoretical Framework

2.1 Hoop Stress

In a conventional space habitat design, the stress experienced by the structure is analogous to a pressurized vessel, described by the following hoop stress equation:

$$\sigma_\theta = \frac{pr}{t_s} \qquad (1)$$

Where σ_θ is the structural stress, p is the centrifugal pressure, r is the radius of the structure, and t_s is the thickness of the structure. Since the outward pressure in a rotating space habitat is due to the weight of the rotating mass, and since weight is the product of mass and acceleration (due to gravity), the equation can be rewritten for a unit area:

$$\sigma_\theta = \frac{Mar}{t_s} \qquad (2)$$

Where M is the rotating mass per unit area and a is centripetal acceleration. All figures in the numerator position are positively correlated with the structural stress. The rotating mass in question can further be separated into structural mass and habitat mass:

$$\sigma_\theta = \frac{(M_s+M_h)ar}{t_s} \qquad (3)$$

This formulation elucidates the reciprocal dynamic between the structural mass M_s and the structural thickness t_s. Specifically, as structural thickness increases (increasing the strength and lowering the stress), the structural mass also increases (increasing the stress), since structural mass and thickness are linearly related.

For any given structural material there is a maximum stress that can be resisted which sets the upper boundary for the σ_θ figure (see section 3.4.1). For a given acceleration and a given mass, there is a maximum rotating habitat radius for any given structural material. To increase the radius beyond that maximum point without increasing the stress beyond the breaking point, additional structural thickness is required, however any additional increase in structural thickness t_s increases the structural mass M_s by the same factor. In other words, an increase in the denominator (structural thickness) is negated with an increase in the numerator (structural mass).

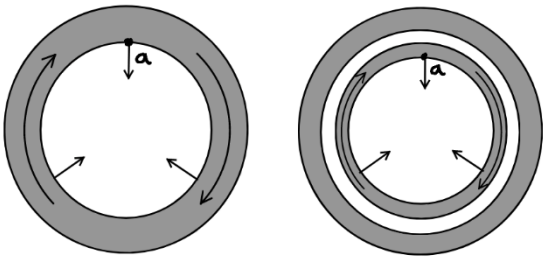

Fig. 1. Conventional (left) vs decoupled (right) rotating habitats

2.2 Decoupling

For this next step, consider that the pressure-resisting structure can be separated from the rotating habitat. Let us further consider that the structure can remain stationary while the habitat is able to rotate (see Fig. 1). This removes the M_s figure from the equation since the

structural mass no longer has any rotational weight, leaving the following:

$$\sigma_\theta = \frac{M_h a r}{t_s} \qquad (4)$$

This equation is notably different from the previous one in that an increase in the value of t_s no longer has any impact on the numerator. In other words, increasing the structural thickness can effectually reduce the stress σ_θ experienced by the structure. Under this paradigm, an increase in the radius can always be cancelled out by an increase in thickness. Effectively, this means that the radius is unlimited, so long as the structural thickness continues to increase in kind.

3. Technology

Decoupling the rotating habitat from the structure supporting it requires the removal of friction that would otherwise exist between the habitat and the structure, in the same way that lubricant reduces the friction between two mechanical components. There are several methods of reducing friction for differential velocity, including lubricant, wheels/bearings, fluid cushions, and magnetic levitation. Each method has operating parameters that must be met for successful operation, one of the most important being the speed of the differential velocity. No amount of lubricant will withstand the velocities involved in even moderately sized rotating habitats for long [9]. Wheels and bearings have a maximum rotational velocity they can support without tearing themselves apart from hoop stress, and the friction experienced (however small) by the contact surfaces compounds over time as the habitat is in a constant state of motion. Depending on the fluid used, a fluid cushion may have varying tolerances for differential velocity, however the slowing friction (even if non-destructive) reduces the economy of the system at moderately large scales and evaporation due to exposure of the fluid to the vacuum of space raises even more engineering challenges. Magnetic levitation, by contrast, is uniquely suited to the environment of space as it can operate free of any material contact, at a distance, and at practically unlimited velocities. Not all magnetic levitation technologies are the same, however; each have their own advantages and drawbacks.

3.1 The Three Pillars of Propelled Magnetic Levitation

3.1.1 Lift

A core requirement of propelled magnetic levitation, lift is responsible for counteracting the gravitational weight (or centrifugal weight in the case of a rotating habitat). To provide lift, sufficient magnetic force must be generated to counteract this weight. If the magnetic force is insufficient, the rotating inner ring will contact the outer structural ring, causing (possibly catastrophic) damage as well as counteractive rotational acceleration in both rings. In the context of a decoupled habitat, this lifting force need only center the habitat radially as it rotates and does not strictly require power, as even passive magnets can provide lift by themselves without any power input.

3.1.2 Stability

Earnshaw's theorem proves that a static, hard magnet cannot be stably levitated within any arrangement of magnetic fields [10]. This instability is a challenge for any guided magnetic levitation system as the levitating portion can only stay aloft if it remains squarely over the lift-providing field. A stability-providing system would function either through active intervention or passive intervention via a physical feedback system. Physical feedback systems carry the advantage of functioning without active power and/or control systems as opposed to active intervention which requires power and/or control systems to function.

3.1.3 Propulsion

Accelerating and maintaining speed are necessary for any levitated conveyance, as the system will inevitably change via entropy or human intervention. On terrestrial Maglev trains, this may constitute speed changes due to stopping at stations or counteracting air friction. In a decoupled rotating space habitat, this may constitute accommodating changes in rotating mass as well as any potential magnetic drag. For such a rotating habitat, a combination of magnetic acceleration and thrusters may be indicated depending on the circumstances.

3.2 Types of Magnetic Levitation

3.2.1 Electrodynamic Suspension

Electrodynamic suspension is a consequence of Faraday's law of induction, and allows simple, conductive materials to be suspended above one or many conductive coils coursing with alternating current. The changing magnetic field produced by the alternating current in the source coil induces an opposite magnetic field in the levitated material, resulting in a magnetic repulsion. Using clever arrangements of the source coils, a homogenous object can even be stable in one or more directions.

This technology has previously been proposed for use in Maglev trains by Professor Eric Laithwaite [11, 12], though this specific method has yet to be commercialized. While the literature offers no definitive explanations for its limited adoption, likely factors include the substantial power required for inductive levitation and the heat generated in the target material via eddy currents. Such drawbacks make inductive levitation an unlikely candidate for use in space where power is finite and heat dissipation is difficult at large scales.

3.2.2 Flux Pinning Levitation

Closely related to the Meisner Effect, flux pinning is the phenomenon observed in Type-II superconducting materials, wherein the magnetic field lines are pinned within the flux vortices of the material in the presence of moderate-intensity magnetic fields. The result of this phenomenon is the ability of the superconducting material (as well as any connected object) to levitate with respect to another magnetic field-producing object. While this phenomenon has been demonstrated and documented by numerous individuals, it remains a demonstration material rather than a commercial one, despite the successful demonstration of a test vehicle for a Brazilian project known as MagLev-Cobra [13]. This is partly due to the high fabrication cost of high temperature superconductors such as YBCO. Most critically however, superconductivity cannot persist in the presence of magnetic fields that exceed a certain critical field strength [14]. Were it not for these drawbacks, magnetic levitation due to the Meisner Effect would be an ideal anti-friction solution for high-differential-velocity objects.

3.2.3 Electromagnetic Suspension

Using electromagnets and a feedback loop control system, an object can be stably suspended via attractive magnetic forces [15]. This technique works only with magnetic attraction however, as attraction is naturally self-centering whereas magnetic repulsion is not. The difference is analogous to hanging by a pole vs balancing on top of a pole (see Fig. 2). This method of levitation relies on sensor input being processed, forming the inputs to electromagnets (either through varying their power or through pulse width modulation (PWM)) such that the average attractive force from the electromagnets to the target is balanced by the acceleration of the system (usually gravity). This method suffers from the necessarily large power consumption of the electromagnets as well as the critical failure modes of power loss and/or loss of active control systems.

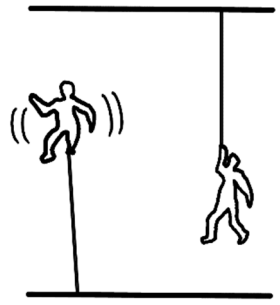

Fig. 2. Self-centering stability

3.2.4 Spin-Stabilized Levitation

One alternative for a low-tech levitation method is spin-stabilized levitation, popularized in the early 1990s by the toy known as the Levitron, though the invention came nearly a decade prior [16]. This is the phenomenon wherein stable levitation can be achieved by spinning a magnet over another, specifically-shaped magnetic field such that the angular momentum and gyroscopic procession provide the damping and stability required to overcome the consequences of Earnshaw's Theorem (see section 3.1.2). Spin-stabilized levitation is another phenomenon that has been extensively demonstrated and documented by numerous individuals. Under this paradigm, so long as the rotating magnet continues to spin with sufficient speed, the magnet will continue to levitate stably in the parent magnetic field. The reasons for this stability are the angular momentum afforded by the rotation as well as the procession of the magnet within the magnetic field [17]. While it's not clear at this point whether reasonable procession will occur with a scaled-up version of this sort of levitated system, the resistance to changes in orientation afforded by a high angular momentum would undoubtedly increase the stability of such a rotating habitat. Angular momentum L is the product of the moment of inertia I and the angular velocity ω as shown in the following equation for angular momentum.

$$L = I\omega \qquad (5)$$

The moment of inertia I of a rotating system is itself the product of the mass m and the square of the radius r.

$$I = Mr^2 \qquad (6)$$

The moment of inertia equation can then be rewritten to illustrate that it is linearly correlated with the mass and angular velocity and is exponentially correlated with the radius.

$$L = Mr^2\omega \qquad (7)$$

This means that a rotating habitat might have rotational stability at a low angular velocity provided it has a sufficiently large radius and/or mass. It is worth noting that this gyroscopic effect may likely work in tandem with other methods of magnetic levitation and is well-suited to rotating habitats, even as a secondary stabilizing phenomenon.

In conventional demonstrations of this effect without active rotational acceleration, air friction eventually slows the object's rate of rotation to the point that it can no longer stably levitate within the parent magnetic field. In the context of rotating habitats (ie, outer space), this air friction is not present.

3.2.5 Null Flux Coil Suspension

An advanced technique for magnetic levitation currently being used for Maglev trains, high power

superconducting coils used together with cross-coupled null flux coils (NFC) carries great potential. When cooled to below their critical temperature, large superconducting coils can be injected with a high current that does not dissipate. This current generates a powerful magnetic field that is directed at a series of NFCs. The movement of the superconducting coils across the static NFCs induces a magnetic field in the NFCs which provides a passive lifting and centering force [18]. So long as the superconducting coils remain in motion and below their critical temperature, the stabilizing effects will persist indefinitely, even in the event of power interruption. The unique environment of space makes the cooling of the superconducting coils below their critical temperature highly energy efficient, a positive indication for the use of this technology in space, an indication noted in research by Jevtovic [19].

Table 1. Levitation method comparison

	Failure Resistant	Energy Efficient	Cost Effective
Electrodynamic Suspension	✗	✗	✗
Flux Pinning Levitation	✗	✓	✗
Electromagnetic Suspension	✗	✗	✗
Spin-Stabilized Levitation	✗	✓	✓
Null Flux Coil Suspension	✓	✓	✓

3.3 Suggested Implementation

The most appropriate type of magnetic levitation to use for a decoupled rotating space habitat should be as relatively failure-resistant, energy efficient, and cost effective as possible (see Table 1*). For these reasons, null flux coil suspension stands out as particularly well-suited to decoupled rotating habitats.

3.4 Structure

3.4.1 Legacy Conceptions

Proposals for structural material to be used in rotating habitats vary widely depending on the scale of said habitat. For moderately sized habitats, steel may be sufficient. For larger habitats, stronger and lighter materials are required. For still larger habitats, there is no material known that can withstand the hoop stress generated by the rotating mass. The largest a rotating system can be is limited by the ultimate tensile strength of the structural material and is known as the breaking length.

To find the breaking length for a given material, we must start with the hoop stress equation (see equation 1), where σ_θ is the hoop stress, p is the outward pressure, r is the radius, and t_s is the thickness of the structure. Since the breaking length is a property of the material itself, the thickness t_s can be set to 1 meter and effectively abstracted away.

$$\sigma_\theta = pr \qquad (8)$$

Additionally, the value for hoop stress σ_θ can be set to the material's ultimate tensile strength F_{tu} since it is at this ultimate tensile strength where the maximum radius can be achieved.

$$F_{tu} = pr \qquad (9)$$

Finally, since the Pascal (Pa) is defined as 1N/m^2 and the Newton (N) is defined as $1\text{kg}\cdot\text{m/s}^2$, the pressure p in Pascals is equal to the density d (in kg/m^3) of the structural material multiplied by the centripetal acceleration a (in m/s^2)†. With these constraints, the equation can be refactored and rearranged to the following.

$$F_{tu} = (da)r \quad \Rightarrow \quad r = \frac{F_{tu}}{da} \qquad (10)$$

For Earth-analogue gravity simulation, the acceleration a can be set to 9.8m/s^2. This modification yields an equation where the breaking length in radius r can be found using only the structural material properties of ultimate tensile strength F_{tu} (in Pa) and density d (in kg/m^3). This can be extended to the diameter D of the habitat by multiplying by a factor of 2.

$$r = \frac{F_{tu}}{9.8d} \quad \Rightarrow \quad D = \frac{2F_{tu}}{9.8d} \qquad (11)$$

As shown in the previous equations, the breaking lengths are positively correlated with the ultimate tensile strength F_{tu} and are inversely correlated with the density d. The following table shows the breaking lengths for

* Table 1 provides a coarse comparison based on the discussion in section 3.2. A more detailed comparative analysis should be conducted to verify the relative failure resistance, energy efficiency, and cost effectiveness of the methods of levitation

† The density in kg/m^3 is applicable in this instance as the thickness of the structure has been abstracted to 1 meter, so a notional square meter of structural material will have approximately the same mass (kg/m^2) as the density of the structural material in kg/m^3. This is only an approximation as the actual mass will depend slightly on the radius of the hoop; the same arc length of 1 meter will have a greater arc angle at smaller radii than larger radii, so the extruded square meter of structure resembles only a skewed cube rather than a perfect one.

some common structural materials cited for use in rotating habitats.

Table 2. Breaking lengths for structural materials

Material	Density, d (kg/m^3)	Ultimate Tensile Strength, F_{tu} (MPa)	Breaking Diameter, D (km)
Nylon	1,150	78	13.84
Stainless Steel	7,930	620	15.96
Titanium	4,510	1,300	55.8
Carbon Fiber	1,750	1,600	186
Kevlar	1,440	3,620	513
Zylon	1,560	5,800	759
Carbon Nanotubes	1,340	62,000	9,443
Graphene	1,000	50,000	10,204

3.4.2 Extensive Material Viability

As described in the decoupling equation (see equation 4), an increase in habitat radius can be accommodated by increasing the non-rotating structural thickness without increasing the structural stress. Consequentially, the feasibility of a habitat having an enormous radius is not contingent on a structural material with a high strength-to-weight ratio; rather, many common structural materials are viable for large-radius rotating habitats. The feasibility of using common structural materials for habitats of any given radius depends on whether the amount of material required 1) rivals the available material in the solar system, or 2) is massive enough to generate enough gravity to disturb the habitat system. Regarding consideration 1, such a situation could come about if the radius is tremendously large and/or the structural material is especially weak in tension. For consideration 2, a sufficiently weak structural material may contribute gravity at a higher rate than structural strength, which has the effect of slowly augmenting the rotational gravity with mass gravity; if said mass gravity overpowers the integrity of the structure, the stability of the habitat may not be feasible. These two considerations are boundary conditions and are not likely to be observed with established structural materials.

To illustrate this, consider the largest conceivable rotating structures that can provide a centripetal acceleration of 9.8m/s^2, noted in Table 2. Of these, graphene provides the largest diameter of 10,204 kilometers. Practically speaking however, additional, non-structural habitat mass must be included for this to resemble an actual habitat. Assuming an additional habitat mass of 10 metric tonnes per square meter and a structural thickness of 100 meters, the maximum diameter drops to 9,276 kilometers. If constructed as a decoupled habitat instead, the same diameter could be achieved with a structural thickness of only 9.09 meters, less than 10% than that of the conventional habitat. Moreover, if the same 100-meter structural thickness were used in a decoupled habitat, the diameter could increase to 102,040 kilometers, 11 times larger than the conventional habitat*. This illustrates the degree to which decoupled habitats are more structurally efficient than their conventional counterparts.

Considering the same example, a diameter of 9,276 kilometers can be achieved using a thickness of 284 meters of carbon fiber, 734 meters of stainless steel, or even 7.6 kilometers of ordinary printer paper (though such a material would never be used for this purpose). This illustrates that the structural material for extremely large rotating habitats need not be a matter of structural technology but could instead be a matter of structural quantity.

The feasibility of tremendously large rotating habitats using only common structural materials contradicts the long-held belief that advanced materials are required for such endeavours. In fact, using common structural materials, a decoupled habitat can plausibly be constructed with a radius that rivals any conventional rotating habitat design using advanced (even theoretical) structural materials.

3.5 Counter-rotation

In a decoupled rotating habitat system, the inner rotating ring rotates within the static outer ring, however at the time of construction the inner ring would not yet be rotating. To spin-up the inner ring, there are two main methods that can be used: conventional thrust and magnetic propulsion. Conventional thrust would involve using an array of thrusters to rotationally accelerate the inner ring. This is likely the only method available for spinning-up conventional rotating habitats. Magnetic propulsion would involve magnetically propelling the inner ring against the outer ring and would not be applicable to conventional rotating habitats. The magnetic propulsion method imparts angular momentum on the inner ring; however, it has the undesirable side effect of imparting an equal and opposite angular momentum on the outer ring, or counter-rotation (see Fig. 4). Since any rotation of the outer ring reduces the effective structural strength of the outer ring, the counter-rotation caused by the magnetic propulsion of the inner ring must be neutralized.

* The precise performance increase of decoupled habitats over their conventional counterparts is not a fixed factor, and instead depends on the interplay between the properties of the structural material, the size of the habitat, and the amount of non-structural mass.

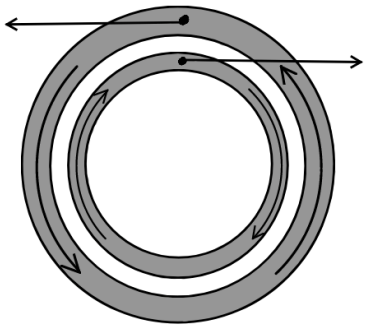

Fig. 4. Unmitigated counter-rotation

One way to neutralize counter-rotation is to use conventional thrust on the outer ring. An array of thrusters on the outer ring can counteract the undesired angular momentum of the outer ring[*]. This method resembles the conventional thrust method used to accelerate the inner ring; however, this method would use even more total energy (magnetic propulsion plus thrust) to mitigate the counter-rotation than simply accelerating the inner ring only (see Fig. 5). Using conventional thrust on the outer ring may still be preferable for larger habitats where it may be impractical to direct the propellant of the thrusters on the inner ring in a way that does not intersect with the inner ring downstream. By contrast, the propellant of thrusters located on the outer ring would not intersect with the outer ring.

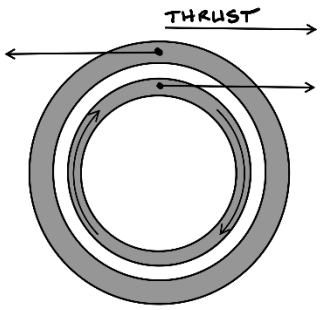

Fig. 5. Thrust compensation

To limit the effect of counter-rotation, the outer ring could be tethered to one or more massive objects; in this way, the angular momentum transferred to the outer ring would be shared with the more massive object(s), which could subsequently be released after the spin-up is completed (see Fig. 6). These massive objects could be a large asteroid, a small moon, or any other object that is both sufficiently massive enough to store a significant portion of the generated inertia and is small enough that the gravitational effects do not interfere with the integrity of the rotating habitat.

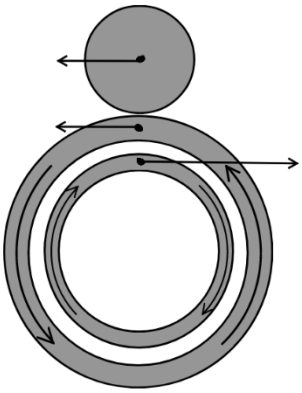

Fig. 6. Mass tethering

One way to completely neutralize the counter-rotation of the outer ring (requiring no conventional thrust) would be to construct two rotating habitats at the same time (twinned habitats). In this case, the outer rings of two rotating habitats can be attached so that the rings resemble a ‘figure 8’. As they magnetically propel their respective inner rings (in opposite directions), the counter-rotation transferred to each outer ring is cancelled by that of the other ring (see Fig. 7).

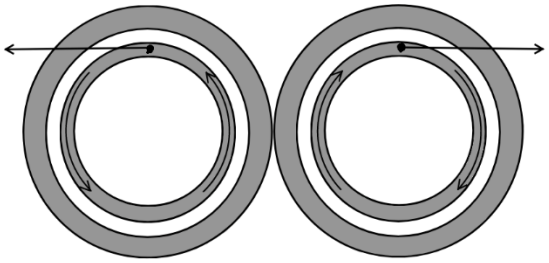

Fig. 7. Twinned habitats

4. Practical Model Validation

To validate the concept of the decoupled orbital using a practical model, the model must demonstrate a resistance to stress induced by either an increased radius, angular velocity, or mass, using a non-rotating support structure. By doing so, the model would demonstrate that the non-rotating structure can supplement the tensile strength of the rotating habitat, thus bypassing the breaking length limitation.

4.1 Method

The practical model uses magnetic force to impart structural cohesion in the form of a static array of

[*] It should be noted that the term “thrusters” is used in this context to connote a device that expels propellant at high velocities. This could include chemical engines, ion thrusters, nuclear engines, or even magnetically propelled projectiles, if deemed suitable to the purpose.

neodymium magnets. There are five main components to the experimental setup: the base, the motor, the rotor head, the outer ring, and the inner ring (see Fig. 8). The base is a sturdy annular platform, having a hole in the center and a raised perimeter. The motor is a small electric motor with a hexagonal shaft and is nested in the hole of the base. The motor is controlled via a separate microcontroller. The rotor head is a spool-shaped component and is inserted onto the shaft of the motor. The outer ring sits on top of the raised lip of the base and its inner face is lined with magnets, each having their north pole facing inward. The inner ring is comprised of three sections, each sweeping a 120° arc. The outer face of each arc is lined with magnets, each having their north pole facing outward. The ends of each arc have small magnets embedded into them, such that the three arcs can be connected to form the complete inner ring. This inner ring is seated around the rotor such that the inner ring is suspended above the base, coplanar with the outer ring*.

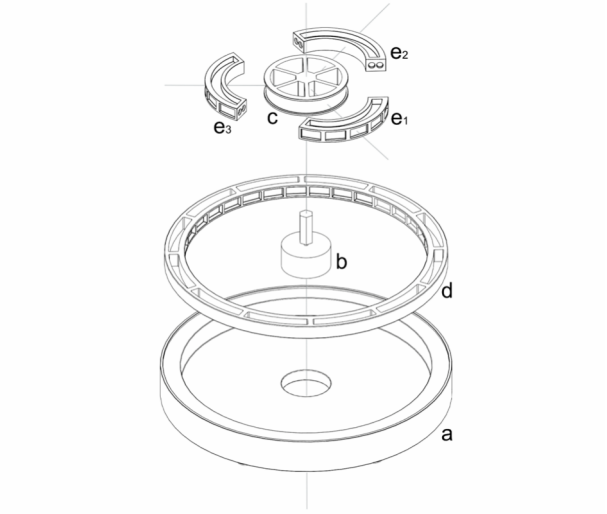

Fig. 8. Experimental apparatus; a) base, b) motor, c) rotor head, d) outer ring, e) inner ring sections

During the experiment, the microcontroller starts the motor spinning at a 20% PWM duty cycle and increases to 100% slowly over the course of one minute and forty-two seconds. The motor rotates the rotor head directly, and friction between the rotor head and the inner ring sets the inner ring rotating. The independent variable is the presence of the outer ring; the outer ring is present for the test series and is absent for the control series. The dependent variable is the angular velocity of the inner ring at failure. A laser tachometer is used to measure the angular velocity (in RPM) of the inner ring via a small strip of reflective tape (see Fig. 9). As the angular velocity of the inner ring increases, the tensile stress also increases until the magnets holding the inner ring together fail and the inner ring arcs are thrown from the apparatus, thus terminating further tachometer readings. The highest angular velocity as measured by the tachometer is recorded.

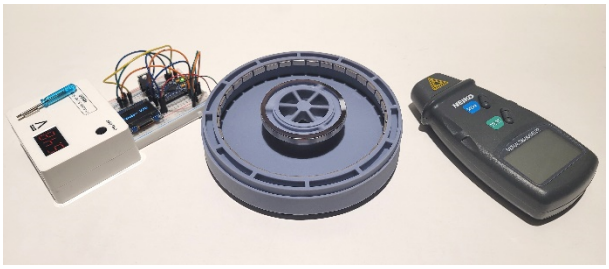

Fig. 9. Experimental setup during testing trial, showing the microcontroller circuit (left), experimental apparatus (center), and laser tachometer (right).

Table 2. Angular velocities (RPM) at failure

Trial	Control	Test
1	685.1	740.7
2	638.1	739.1
3	703.3	706.5
4	706.7	682.2
5	402.9	751.9
6	570.5	695.6
7	586.1	697.1
8	586	682.4
9	563.7	671.3
10	567.5	614.1
11	660.1	689
12	579.5	585.3
13	564.9	685.1
14	655.7	593.9
15	586.5	683.3
Average	**598.8**	**679.4**

4.2 Results

The tachometer readings for the experiment are shown in Table 2. The experiment was conducted 15 times for each of the control and test series. The results show that the test series had an average angular velocity at failure that was over 13% higher than that of the control series. Since the centripetal acceleration, which is a governing factor of rotational hoop stress (see equation 4), scales with the square of the angular velocity (see

* During the design of this experimental apparatus, it was decided that the distance between the inner and outer rings would be roughly the liminal distance where the magnets could be observed to affect one another. While this aids in making the apparatus less sensitive to magnetic torques that could interfere with the results, this of course also reduces the supporting effect of the magnets. Reducing the distance between the inner and outer rings would undoubtedly increase the supporting effect.

equation 12), such an increase in angular velocity implies an effective 28% increase in effective tensile strength.

$$a = \omega^2 r \qquad (12)$$

These results show that the effective tensile strength of a rotating structure can be increased through contact-free magnetic support, thus validating the concept of decoupled rotating habitats.

5. Conclusion

As shown in section 2, a rotating structure is an inefficient liability and limits the feasible size of rotating habitats. By decoupling the rotating habitat from the structure, the size of the habitat can be unlimited as the structural breaking length no longer applies. This decoupling carries the benefits of a more efficient use of structure even for habitats of modest size.

The potential benefits of decoupled rotating habitats are validated by the results of the practical demonstration described in section 4.

Future research should study the use of conventional materials in decoupled rotating habitat design, the thermal dynamics of supercooled, superconducting magnets in space-like environment, and NFC suspension applied to ring-shaped tracks in a weightless environment.

Appendix A (Calculations for Table 2)

Breaking length (diameter) from Equation 11:
$D = \frac{2F_{tu}}{9.8d}$

Calculation for Nylon:
$F_{tu} = 78\ MPa = 78{,}000{,}000\ Pa$
$d = 1{,}150\ m/s^2$
$D = \frac{(2)(78{,}000{,}000)}{(9.8)(1{,}150)} = \frac{156{,}000{,}000}{11{,}270} = 13{,}842\ m \cong 13.84\ km$

Calculation for Stainless Steel:
$F_{tu} = 620\ MPa = 620{,}000{,}000\ Pa$
$d = 7{,}930\ m/s^2$
$D = \frac{(2)(620{,}000{,}000)}{(9.8)(7{,}930)} = \frac{1{,}240{,}000{,}000}{77{,}714} = 15{,}956\ m \cong 15.96\ km$

Calculation for Titanium:
$F_{tu} = 1{,}300\ MPa = 1{,}300{,}000{,}000\ Pa$
$d = 4{,}510\ m/s^2$
$D = \frac{(2)(1{,}300{,}000{,}000)}{(9.8)(4{,}510)} = \frac{2{,}600{,}000{,}000}{44{,}198} = 58{,}826\ m \cong 55.82\ km$

Calculation for Carbon Fiber:
$F_{tu} = 1{,}600\ MPa = 1{,}600{,}000{,}000\ Pa$
$d = 1{,}750\ m/s^2$
$D = \frac{(2)(1{,}600{,}000{,}000)}{(9.8)(1{,}750)} = \frac{3{,}200{,}000{,}000}{17{,}150} = 186{,}589\ m \cong 187\ km$

Calculation for Kevlar:
$F_{tu} = 3{,}620\ MPa = 3{,}620{,}000{,}000\ Pa$
$d = 1{,}440\ m/s^2$
$D = \frac{(2)(3620{,}000{,}000)}{(9.8)(1{,}440)} = \frac{7{,}240{,}000{,}000}{14{,}112} = 513{,}039\ m \cong 513\ km$

Calculation for Zylon:
$F_{tu} = 5{,}800\ MPa = 5{,}800{,}000{,}000\ Pa$
$d = 1{,}560\ m/s^2$
$D = \frac{(2)(5{,}800{,}000{,}000)}{(9.8)(1{,}560)} = \frac{11{,}600{,}000{,}000}{15{,}288} = 758{,}765\ m \cong 759\ km$

Calculation for Carbon Nanotubes:
$F_{tu} = 62{,}000\ MPa = 62{,}000{,}000{,}000\ Pa$
$d = 1{,}340\ m/s^2$
$D = \frac{(2)(62{,}000{,}000{,}000)}{(9.8)(1{,}340)} = \frac{124{,}000{,}000{,}000}{13{,}132} = 9{,}442{,}583\ m \cong 9{,}443\ km$

Calculation for Graphene:
$F_{tu} = 50{,}000\ MPa = 50{,}000{,}000{,}000\ Pa$
$d = 1{,}000\ m/s^2$
$D = \frac{(2)(50{,}000{,}000{,}000)}{(9.8)(1{,}000)} = \frac{100{,}000{,}000{,}000}{9{,}800} = 10{,}204{,}082\ m \cong 10{,}204\ km$

Appendix B (Calculations for Section 3.4.2)

Modification of Equation 3:
$F_{tu} = \frac{(M_s + M_h)ar}{t_s} \iff r = \frac{F_{tu}t_s}{(M_s + M_h)a}$

Modification of Equation 4:
$F_{tu} = \frac{(M_h)ar}{t_s} \iff t_s = \frac{(M_h)ar}{F_{tu}}$

Assumptions:
$M_h = 10{,}000\ kg$
$a = 9.8\ m/s^2$

Conventional rotating habitat (Graphene):
$F_{tu} = 50{,}000{,}000{,}000\ Pa$
$d = 1{,}000\ kg/m^3$
$t_s = 100\ m$
$M_s = t_s d = (100\ m)(1{,}000\ kg/m^3) = 100{,}000\ kg/m^2$
$r = \frac{F_{tu}t_s}{(M_s + M_h)a} = \frac{(50{,}000{,}000{,}000)(100)}{(100{,}000\ + 10{,}000)(9.8)} = \frac{5{,}000{,}000{,}000{,}000}{1{,}078{,}000} = 4{,}638{,}219\ m = 4{,}638\ km$
$D = 2r = (2)(4{,}638) = 9{,}276\ km$

Decoupled rotating habitat (Graphene):
$r = 4{,}638{,}219\ m$
$F_{tu} = 50{,}000{,}000{,}219\ Pa$
$t_s = \frac{(M_h)ar}{F_{tu}} = \frac{(10{,}000)(9.8)(4{,}638{,}219)}{50{,}000{,}000{,}000} = \frac{454{,}545{,}462{,}000}{50{,}000{,}000{,}000} = 9.09\ m$

Decoupled rotating habitat (Carbon Fiber):
$r = 4{,}638{,}219\ m$
$F_{tu} = 1{,}600{,}000{,}000\ Pa$
$t_s = \frac{(M_h)ar}{F_{tu}} = \frac{(10{,}000)(9.8)(4{,}638{,}219)}{1{,}600{,}000{,}000} = \frac{454{,}545{,}462{,}000}{1{,}600{,}000{,}000} = 284\ m$

Decoupled rotating habitat (Stainless Steel):
$r = 4{,}638{,}219\ m$
$F_{tu} = 620{,}000{,}000\ Pa$
$t_s = \frac{(M_h)ar}{F_{tu}} = \frac{(10{,}000)(9.8)(4{,}638{,}219)}{620{,}000{,}000} = \frac{454{,}545{,}462{,}000}{620{,}000{,}000} = 733\ m$

Decoupled rotating habitat (Printer Paper):
$r = 4{,}638{,}219\ m$
$F_{tu} = 60{,}000{,}000\ Pa$
$t_s = \frac{(M_h)ar}{F_{tu}} = \frac{(10{,}000)(9.8)(4{,}638{,}219)}{60{,}000{,}000} = \frac{454{,}545{,}462{,}000}{60{,}000{,}000} = 7{,}576\ m = 7.6\ km$

References

[1] T. W. Hall, "Artificial Gravity: Why Centrifugal Force is a Bad Idea," in *AIAA ASCEND 2020*, Virtual, 2020.

[2] K. Tsiolkovsky, "The Rocket into Cosmic Space," *Na-ootchnoye Obozreniye,* Science Survey, Moscow*,* 1903.

[3] W. von Braun, "Crossing the Last Frontier," *Collier's,* pp. 24-29, 72, 74, 22 March 1952.

[4] H. Noordung, The Problem of Space Travel - The Rocket Motor, Berlin: Richard Carl Schmidt, 1928.

[5] S. Kubrick, Director, *2001: A Space Odyssey.* [Film]. United Kingdom: Stanley Kubrick Productions, 1968.

[6] National Aeronautics and Space Administration, Space Settlements: A Design Study, Washington: Scientific and Technical Information Office, National Aeronautics and Space Administration, 1977.

[7] I. M. Banks, Consider Phlebas, London: Macmillan, 1987.

[8] L. Nivin, Ringworld, New York: Ballantine Books, 1970.

[9] H. Czichos, "Failure criteria in thin film lubrication— the concept of a failure surface," *Tribology,* vol. 7, no. 1, pp. 14-20, 1974.

[10] S. Earnshaw, "On the Nature of the Molecular Forces which regulate the Constitution of the Luminiferous Ether," *Transactions of the Cambridge Philosophical Society,* vol. 7, pp. 97-112, 1842.

[11] E. Laithwaite, "Linear induction motors for high-speed vehicles," *Electronics and Power,* vol. 15, no. 7, pp. 230-233, 1969.

[12] J. Eastham and E. Laithwaite, "Linear induction motors as ‘electromagnetic rivers’," *Electronics and Power,* vol. 20, no. 22, p. 1108, 1974.

[13] L. Mattos, E. Rodriguez, F. Costa, G. Sotelo, R. de Andrade Jr. and R. Stephan, "MagLev-Cobra Operational Tests," *IEEE Transactions on Applied Superconductivity,* vol. 26, no. 3, pp. 1-4, 2016.

[14] V. Kogan and R. Prozorov, "Critical fields of superconductors with magnetic impurities," *Physical Review B,* vol. 106, no. 5, 2022.

[15] K.-J. Kim, H.-S. Han, C.-H. Kim and S.-J. Yang, "Dynamic Analysis of a Maglev Conveyor Usingan EM-PM Hybrid Magnet," *Journal of Electrical Engineering and Technology,* vol. 8, no. 6, pp. 1571-1578, 2013.

[16] R. M. Harrigan, "Magnetic Levitation Device and Method". USA Patent 5,404,062, 17 Feb. 1983.

[17] M. D. Simon, L. O. Heflinger and S. Ridgeway, "Spin stabilized magnetic levitation," *American Journal of Physics,* vol. 65, no. 4, pp. 286-292, 1997.

[18] J. He, D. Rote and H. Coffey, "Electrodynamic forces of the cross-connected figure-eight null-flux coil suspension system," in *Maglev '93*, Argonne, 1993.

[19] P. Jevtovic, "Electrodynamic Centrifuge for Space Modules with Artificial Gravity," in *ASCEND 2021, American Institute of Aeronautics and Astronautics*, Las Vegas, 2021.